

Baryonic torii: Toroidal baryons in a generalized Skyrme model

Sven Bjarke Gudnason¹ and Muneto Nitta²

¹*Nordita, KTH Royal Institute of Technology and Stockholm University, Roslagstullsbacken 23, SE-106 91 Stockholm, Sweden*

²*Department of Physics, and Research and Education Center for Natural Sciences, Keio University, Hiyoshi 4-1-1, Yokohama, Kanagawa 223-8521, Japan*

(Received 6 November 2014; published 20 February 2015)

We study a Skyrme-type model with a potential term motivated by Bose–Einstein condensates (BECs), which we call the BEC Skyrme model. We consider two flavors of the model: the first is the Skyrme model, and the second has a sixth-order derivative term instead of the Skyrme term, both with the added BEC-motivated potential. The model contains toroidally shaped Skyrmions, and they are characterized by two integers P and Q , representing the winding numbers of two complex scalar fields along the toroidal and poloidal cycles of the torus, respectively. The baryon number is $B = PQ$. We find stable Skyrmion solutions for $P = 1, 2, 3, 4, 5$ with $Q = 1$, while for $P = 6$ and $Q = 1$, it is only metastable. We further find that configurations with higher $Q > 1$ are all unstable and split into Q configurations with $Q = 1$. Finally we discover a phase transition, possibly of first order, in the mass parameter of the potential under study.

DOI: 10.1103/PhysRevD.91.045027

PACS numbers: 11.27.+d, 12.39.Dc

I. INTRODUCTION

Half a century has passed since Skyrme proposed [1] that Skyrmions characterized by the topological charge $\pi_3(S^3) \simeq \mathbb{Z}$ describe nucleons in the pion effective field theory or the chiral Lagrangian [2], where the Skyrme term, i.e. quartic in derivatives, is needed to stabilize Skyrmions against shrinkage. Although nucleons are now known to be bound states of quarks, the idea of the Skyrme model is still attractive. In fact, the Skyrme model is still valid as a low-energy description of QCD, has only a small number of parameters, and is, for instance, used also in holographic QCD [3,4].

Meanwhile in condensed matter physics, considerable efforts have been made recently to realize stable three-dimensional Skyrmions in two-component Bose–Einstein condensates (BECs) [5–8] (see Ref. [9] for a review of two-component BECs). In Ref. [8], the creation of a Skyrmion is proposed to be a consequence of the annihilation of a brane and an antibrane [10]. At strong coupling, these systems reduce to the SU(2) principal chiral model, but the existence of Skyrmions is elusive due to the lack of the Skyrme term (or an even higher-order derivative term) [11]. One interesting feature in these systems is that a potential term, breaking the SU(2) symmetry, is present, which deforms the (would-be) Skyrmion to the shape of a torus [5]. Consequently, the Skyrmion can be interpreted [5,8,12] as a vorton [13–16], that is, a vortex ring in the first component with the second component flowing inside said ring.

In this paper, we consider a Skyrme-like model with a potential term in the form $V = m^2|\phi_1|^2|\phi_2|^2$ which was introduced in our previous papers [17,18] and is motivated by two-component BECs [5,6,8], where we use a notation

of two complex scalar fields $\phi_1(x)$ and $\phi_2(x)$ with the constraint $|\phi_1|^2 + |\phi_2|^2 = 1$ along the lines of two-component BECs. For higher-derivative terms needed to stabilize Skyrmion, we consider either the conventional fourth-order derivative term, i.e. the Skyrme term, or a sixth-order derivative term, which is the baryon charge density squared (see, e.g., Refs. [18–20]); for a short-term notation, we will call the first case the $2+4$ model and the second case the $2+6$ model. We construct stable Skyrmions which were elusive in two-component BECs in the absence of the Skyrme term or other higher-order derivative terms and find that they take the shape of a torus as two-component BECs. We find that the most general solutions are characterized by two integers P and Q , representing the winding numbers of the scalar fields ϕ_1 and ϕ_2 along the toroidal and poloidal cycles of the torus, respectively, and show that the baryon number or the Skyrmion number of $\pi_3(S^3) \simeq \mathbb{Z}$ is $B = PQ$ (which is also known as the linking number). We explicitly construct stable Skyrmion solutions with $P = 1, 2, 3, 4, 5$ and $Q = 1$, yielding the baryon numbers $B = 1, 2, 3, 4, 5$. We also construct the $P = 6$, $Q = 1$ solution and find that it is metastable, i.e. is energetically prone to decay into two $B = 3$ objects. This turns out to be the case for both the $2+4$ and the $2+6$ models.

The energy and baryon charge distributions of the configuration of $P = 1$ are spherically symmetric in the $2+4$ model, whereas in the $2+6$ model, it is a deformed ball (with a hint of a toruslike shape). The configurations with $P > 1$ are all of toroidal shapes (for both models) when the mass is bigger than a certain critical mass. This is in contrast to the conventional Skyrmions (i.e. without our BEC-motivated potential) for which the configuration of $B = 1$ is spherically symmetric, that of $B = 2$ is toroidal,

and those of $B > 1$ have energy distributions with some point symmetry. We compare our $B = 2$ solutions in the $2 + 4$ and $2 + 6$ models to those of the conventional model (i.e. without the BEC-motivated potential) and find that the energy distribution of the solution in the $2 + 6$ model is a surface of a torus while the energy distributions of the solutions in the $2 + 4$ model and the conventional model are solid torii, i.e. filled torii.

Although the classification of our solutions is given by the integers P and Q , we find that configurations with $Q > 1$ are unstable; that is, a configuration with (P, Q) decays into Q copies of the $(P, 1)$ configuration.

We also note that our configurations can be identified as global analogs of vortons [13–15], that is, twisted closed global vortex strings as in two-component BECs [21]. While vortices in this model are global vortices so that straight vortices have divergent energy per unit length, a closed string has finite energy because of cancellation of vorticity. A vortex in the field ϕ_1 traps the field ϕ_2 in its core and has the U(1) phase modulus of ϕ_2 . The integers Q and P are identified with the winding numbers of the vortex of the ϕ_1 field and of the ϕ_2 field along the ring inside the vortex core, respectively. The identification of the Skyrmions with global vortex rings also explains why configurations with higher $Q > 1$ are unstable. This is because Q is the winding number of the vortex in the field ϕ_1 , and a global vortex with higher winding is unstable to decay as two global vortices repel each other.

Finally we discover a first-order phase transition between the configuration (local minimum) where the Skyrmions have a (discrete) point symmetry and the toroidal configuration (another local minimum) at some critical mass, m_{critical} . For concreteness we carry out this investigation at $B = 3$ where the Skyrmion has tetrahedral symmetry for $m < m_{\text{critical}}$ and has axial symmetry (i.e. it is a torus) for $m > m_{\text{critical}}$. For $m < m_{\text{critical}}$ the toroidal state is metastable, and for $m > m_{\text{critical}}$ the tetrahedral state is metastable. For sufficiently large $m \sim 2m_{\text{critical}}$, the tetrahedral solution becomes unstable, and thus for large m , only the torus exists.

This paper is organized as follows. In Sec. II, we present our model and explain the symmetries and topological structures of the model. In Sec. III, we construct a domain wall and a global vortex which serve as constituents of the torus. Finally, in Sec. IV, we construct toroidal Skyrmions which are the strings wrapped up on a circle, and we further study their stability. The phase transition between the Skyrmions with point symmetry and with axial symmetry is studied in Sec. V. Section VI is devoted to a summary and discussions. In Appendix A, we show that solutions with $P = 1, 2$ and $Q = 2$ are unstable to decay into two configurations of $P = 1, 2$ and $Q = 1$. In Appendix B, we compare our $B = 2$ solutions in the $2 + 4$ and $2 + 6$ models and that in the conventional models (i.e. without the BEC-motivated potential).

II. A SKYRME-LIKE MODEL WITH BEC-MOTIVATED POTENTIAL

We consider the SU(2) principal chiral model with the addition of the Skyrme term and a sixth-order derivative term in $d = 3 + 1$ dimensions. In terms of the SU(2)-valued field $U(x) \in \text{SU}(2)$, the Lagrangian which we are considering is given by

$$\mathcal{L} = \frac{f_\pi^2}{16} \text{tr}(\partial_\mu U^\dagger \partial^\mu U) + \mathcal{L}_4 + \mathcal{L}_6 - V(U), \quad (1)$$

where we use the mostly negative metric and the higher-derivative terms are given by

$$\mathcal{L}_4 = \frac{\kappa}{32e^2} \text{tr}([U^\dagger \partial_\mu U, U^\dagger \partial_\nu U]^2), \quad (2)$$

$$\mathcal{L}_6 = \frac{c_6}{36e^4 f_\pi^2} (\epsilon^{\mu\nu\rho\sigma} \text{tr}[U^\dagger \partial_\nu U U U^\dagger \partial_\rho U U^\dagger \partial_\sigma U])^2. \quad (3)$$

The symmetry of the Lagrangian for $V = 0$ is $\tilde{G} = \text{SU}(2)_L \times \text{SU}(2)_R$ acting on U as $U \rightarrow U' = g_L U g_R^\dagger$. The requirement of a finite-energy configuration, however, spontaneously breaks this symmetry down to $\tilde{H} \simeq \text{SU}(2)_{L+R}$, which in turn acts as $U \rightarrow U' = g U g^\dagger$ so that the target space is $\tilde{G}/\tilde{H} \simeq \text{SU}(2)_{L-R}$. The conventional potential term, i.e. the pion mass term, is $V = m_\pi^2 \text{tr}(2\mathbf{1}_2 - U - U^\dagger)$, which breaks the symmetry \tilde{G} to $\text{SU}(2)_{L+R}$ explicitly.

In this paper, it will prove convenient to use the notation where we express the field U in terms of two complex scalar fields, $\phi^T = (\phi_1(x), \phi_2(x))$, as

$$U = \begin{pmatrix} \phi_1 & -\phi_2^* \\ \phi_2 & \phi_1^* \end{pmatrix}, \quad (4)$$

subject to the constraint

$$\det U = |\phi_1|^2 + |\phi_2|^2 = 1. \quad (5)$$

We further rescale the lengths to be in units of $2/(ef_\pi)$ and energy to be in units of $f_\pi/(2e)$, for which we can write the static Lagrangian density as

$$\begin{aligned} -\mathcal{L} = & \frac{1}{2} \partial_i \phi^\dagger \partial_i \phi \\ & + \frac{\kappa}{4} \left[(\partial_i \phi^\dagger \partial_i \phi)^2 - \frac{1}{4} (\partial_i \phi^\dagger \partial_j \phi + \partial_j \phi^\dagger \partial_i \phi)^2 \right] \\ & + \frac{c_6}{4} (\epsilon^{ijk} \phi^\dagger \partial_i \phi \partial_j \phi^\dagger \partial_k \phi)^2 + V(\phi, \phi^*). \end{aligned} \quad (6)$$

The full symmetry \tilde{G} is not manifest in terms of ϕ , where only $\text{SU}(2)_L$ is manifest but $\text{SU}(2)_R$ is not. The U(1) subgroup generated by σ_3 in $\text{SU}(2)_R$, however, is manifest and acts on ϕ as $\phi \rightarrow e^{i\alpha} \phi$, constituting a U(2) group with $\text{SU}(2)_L$.

The target space (the vacuum manifold with $m = 0$) $M \simeq \text{SU}(2) \simeq S^3$ has a nontrivial homotopy group

$$\pi_3(M) = \mathbb{Z}, \quad (7)$$

which admits Skyrmions as usual. The baryon number (the Skyrme charge) of $B \in \pi_3(S^3)$ is defined as

$$\begin{aligned} B &= -\frac{1}{24\pi^2} \int d^3x e^{ijk} \text{tr}(U^\dagger \partial_i U U^\dagger \partial_j U U^\dagger \partial_k U) \\ &= \frac{1}{24\pi^2} \int d^3x e^{ijk} \text{tr}(U^\dagger \partial_i U \partial_j U^\dagger \partial_k U) \\ &= \frac{1}{4\pi^2} \int d^3x e^{ijk} \phi^\dagger \partial_i \phi \partial_j \phi^\dagger \partial_k \phi. \end{aligned} \quad (8)$$

Instead of the conventional potential term, we consider here a potential term motivated by two-component BECs, given by

$$V(\phi, \phi^*) = \frac{m^2}{8} [1 - (\phi^\dagger \sigma_3 \phi)^2] = \frac{1}{2} m^2 |\phi_1|^2 |\phi_2|^2; \quad (9)$$

see the Appendix of Ref. [17] for a relation to BECs. With this potential, the full symmetry \tilde{G} is explicitly broken down to

$$G = \text{U}(1) \times \text{O}(2) \simeq \text{U}(1)_0 \times [\text{U}(1)_3 \rtimes (\mathbb{Z}_2)_{1,2}]. \quad (10)$$

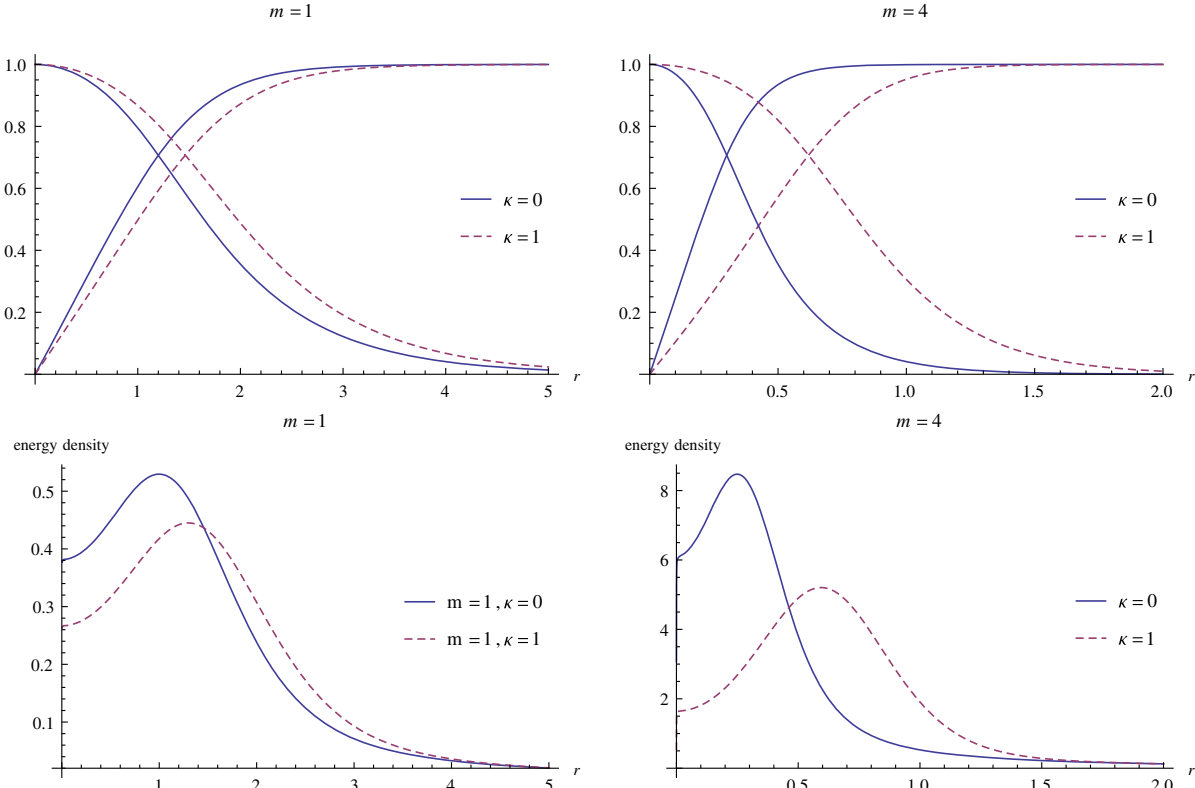


FIG. 1 (color online). Vortex profiles and energy densities for solutions without the Skyrme term $\kappa = 0$ (blue curve) and with the Skyrme term $\kappa = 1$ (dotted red curve) for $m = 1$ (left panels) and $m = 4$ (right panels).

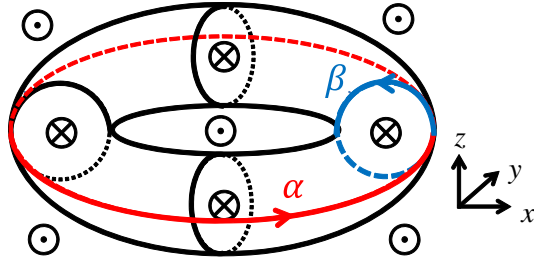


FIG. 2 (color online). The two cycles of the torus. The toroidal and poloidal cycles are denoted by α and β , respectively. The \odot and \otimes denote the vacua in Eq. (14), respectively. The U(1) modulus is twisted P and Q times along the cycles α and β , respectively.

The nontrivial homotopy groups of the vacuum manifold are

$$\pi_0(\mathcal{M}) = \mathbb{Z}_2, \quad \pi_1(\mathcal{M}) = \mathbb{Z}, \quad (17)$$

admitting domain walls and vortices, respectively.

By means of the Hopf map $\vec{n} = \phi^\dagger \vec{\sigma} \phi$, the principal chiral $SU(2)$ model can be mapped to the $O(3)$ nonlinear sigma model with $\vec{n}^2 = 1$ or equivalently the \mathbb{CP}^1 model. The potential term in Eq. (9) is mapped to $V = \frac{m^2}{8}(1 - n_3^2)$, which is referred to as the Ising-type potential in ferromagnets [22]. The \mathbb{CP}^1 model with the same potential is often called the massive \mathbb{CP}^1 model [23–26]. This map can be obtained by coupling a U(1) gauge field to ϕ with common U(1) charges and subsequently taking the strong gauge coupling limit $e \rightarrow \infty$.

III. DOMAIN WALLS AND VORTICES

In this section, we will review the constituents which will be used in the next section in modified or compactified forms.

A. Domain walls

In $d = 1 + 1$ dimensions, a(n) (anti)kink solution interpolating between the two vacua in Eq. (14) is given by

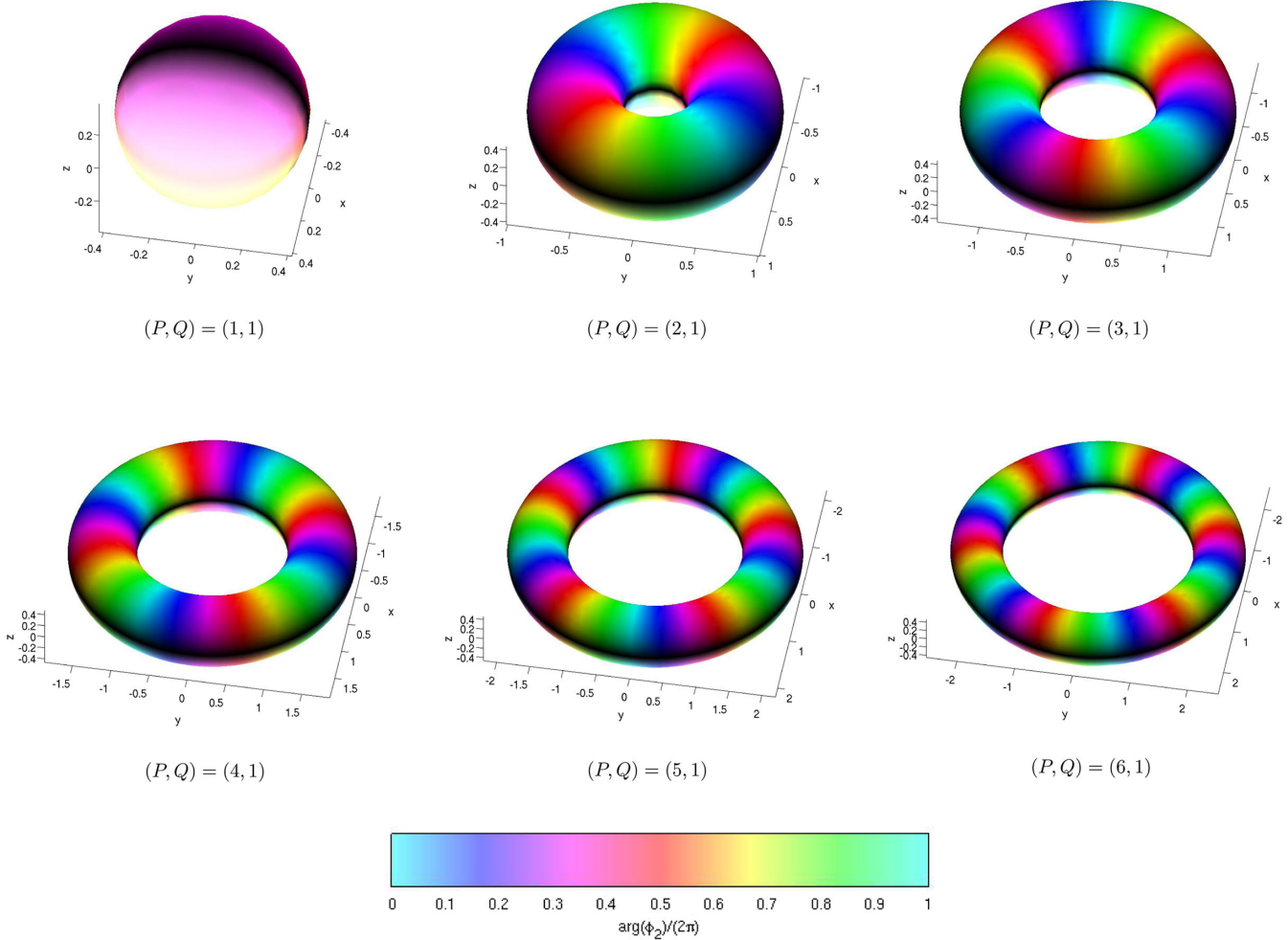


FIG. 3 (color online). Isosurfaces showing the solutions for the $2 + 4$ model, i.e. for $\kappa = 1$ and $c_6 = 0$, at constant baryon charge density equal to half its maximum value. The color represents the phase of the scalar field ϕ_2 , and the lightness is given by $|\Im(\phi_1)|$. The calculations are done on an 81^3 cubic lattice with the relaxation method.

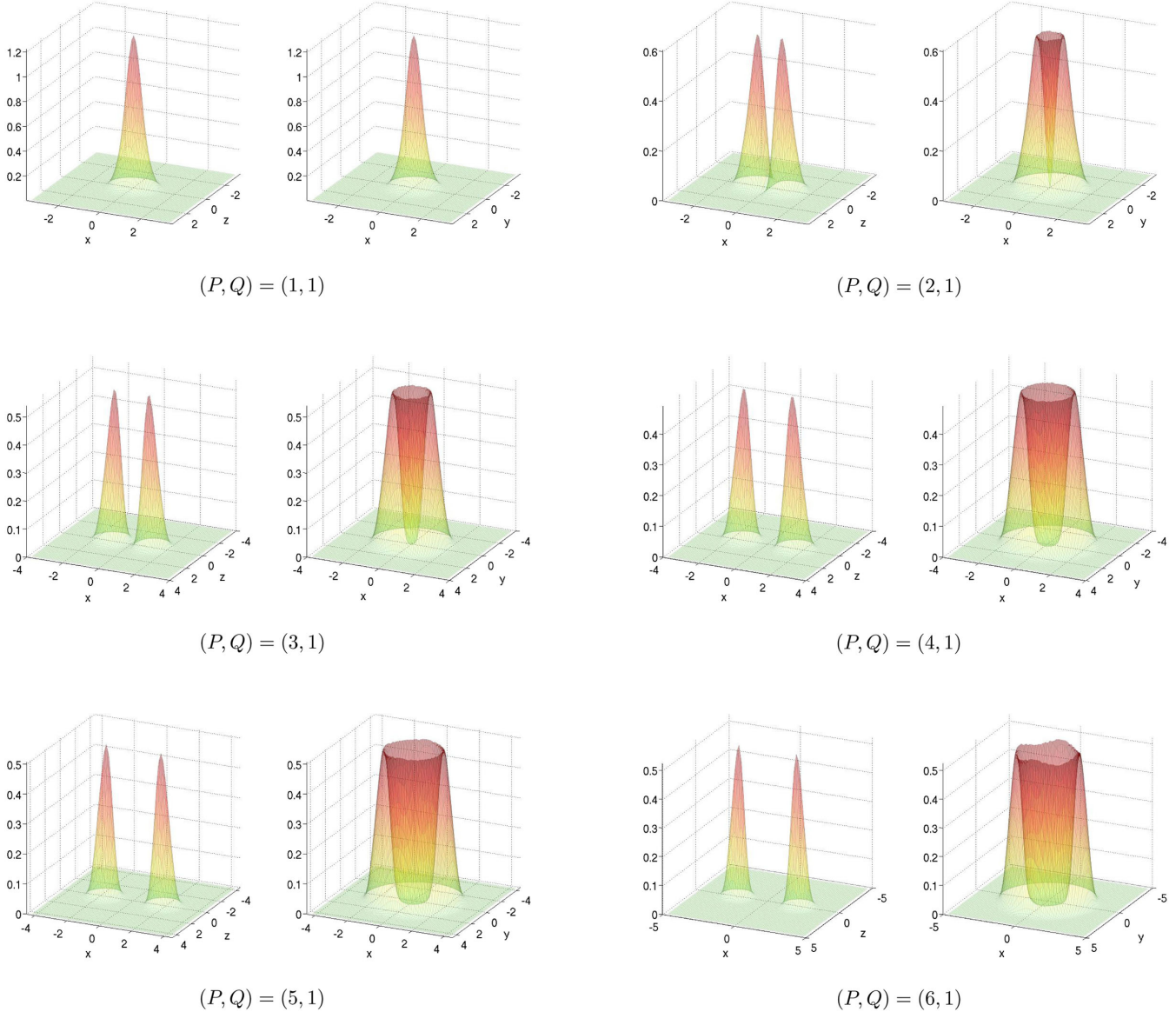


FIG. 4 (color online). Baryon charge density for solutions in the $2 + 4$ model, i.e. with $\kappa = 1$ and $c_6 = 0$, at xz slices (for $y = 0$) and xy slices (for $z = 0$). yz slices are omitted as they are identical to the xz slices by rotational symmetry of the torus. The calculations are done on an 81^3 cubic lattice with the relaxation method.

$$\phi^T = \frac{1}{\sqrt{1 + e^{\pm 2m(x-X)}}} (e^{i\alpha}, e^{\pm m(x-X) + i\beta}), \quad (18)$$

with $X \in \mathbb{R}$ being the translational modulus of the kink. Here α and β are not moduli of the kink but moduli of the vacua in Eq. (14). Note that this solution is (statically) exact in the form given above, even in the presence of the Skyrme or sixth-order derivative term [this can easily be understood as the Skyrme (sixth-order derivative) term is nonzero only when a solution nontrivially depends on two (three) spatial coordinates]. Once waves on top of this static solution are considered, the higher-order derivative terms must be taken into account; see, e.g., Ref. [27].

In the static case, the kink can trivially be extended to a domain line in $d = 2 + 1$ dimensions and to a domain wall in $d = 3 + 1$ dimensions, with a one- and two-dimensional world volume, respectively.

By the Hopf map, the solution (18) is mapped to a kink in the massive $\mathbb{C}P^1$ model [23,24,28]. In that case, the phase difference $\beta - \alpha$ becomes a modulus of the kink.

In the $(3+1)$ -dimensional case, we can think of our toroidal objects in Sec. IV as a domain wall wrapped up on a torus with its S^1 moduli twisted in both world volume directions. It will, however, prove convenient to take a different point of view, as we shall see, namely to consider first a vortex string which is then wrapped up on a circle. In

the next subsection, we therefore review the (global) vortex.

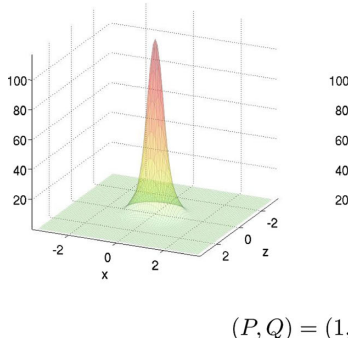
B. Vortices

In $d = 2 + 1$ dimensions the model allows for global vortices. The vortices of ϕ_1 trap or localize ϕ_2 in their cores, and they carry a U(1) modulus being the phase of ϕ_2 .

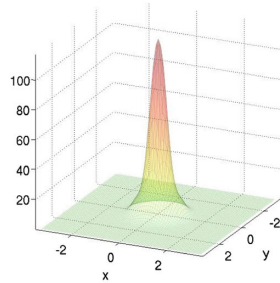
We will now review the global vortex in the nonlinear sigma model with the potential (9); see Ref. [17]. The vortex can be constructed using the Ansatz

$$\phi^T = (\sin f(r)e^{i\varphi+i\alpha}, \cos f(r)e^{i\beta}), \quad (19)$$

where $r \in [0, \infty)$, $\varphi \in [0, 2\pi)$ are polar coordinates in a plane. The constant, α , can be absorbed by a redefinition of



$(P, Q) = (1, 1)$

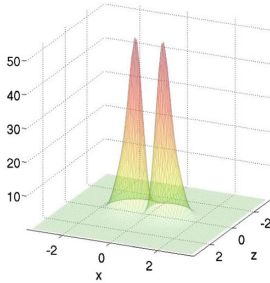


the coordinate φ , while the constant β is a U(1) modulus. This simplifies the Lagrangian density to [17]

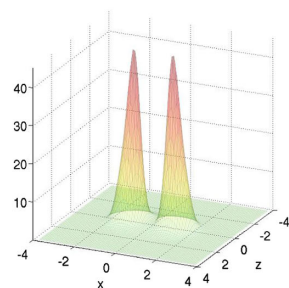
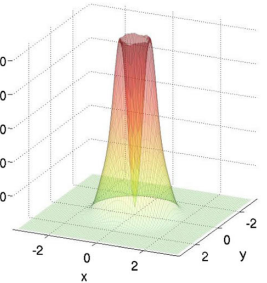
$$-\mathcal{L} = \frac{1}{2}f_r^2 + \frac{1}{2r^2}\sin^2 f + \frac{\kappa}{2r^2}\sin^2(f)f_r^2 + \frac{1}{8}m^2\sin^2(2f), \quad (20)$$

for which the equation of motion reads [17]

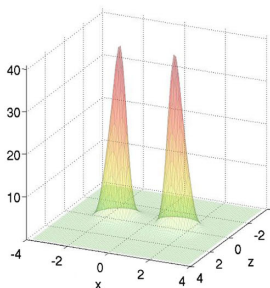
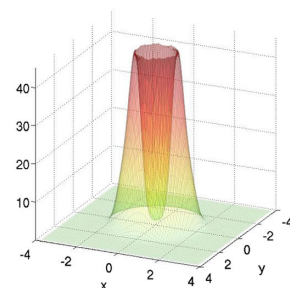
$$f_{rr} + \frac{1}{r}f_r - \frac{1}{2r^2}\sin 2f + \frac{\kappa}{r^2}\sin^2 f \left(f_{rr} - \frac{1}{r}f_r \right) + \frac{\kappa}{2r^2}\sin(2f)f_r^2 - \frac{1}{4}m^2\sin 4f = 0. \quad (21)$$



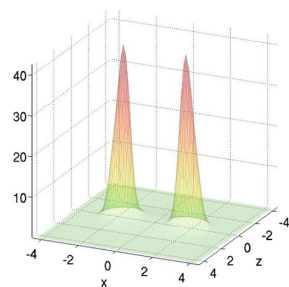
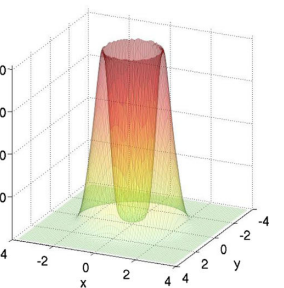
$(P, Q) = (2, 1)$



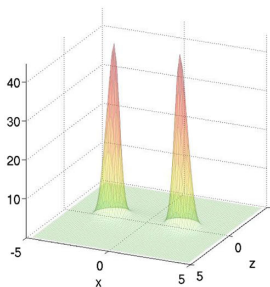
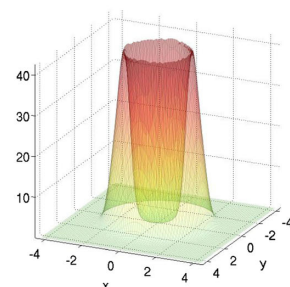
$(P, Q) = (3, 1)$



$(P, Q) = (4, 1)$



$(P, Q) = (5, 1)$



$(P, Q) = (6, 1)$

FIG. 5 (color online). Energy density for solutions in the $2 + 4$ model, i.e. with $\kappa = 1$ and $c_6 = 0$, at xz slices (for $y = 0$) and xy slices (for $z = 0$). yz slices are omitted as they are identical to the xz slices by rotational symmetry of the torus. The calculations are done on an 81^3 cubic lattice with the relaxation method.

TABLE I. Numerically integrated baryon charge and energy (mass) for the solutions in the $2 + 4$ model. Stability is observed for the first five solutions, while $P = 6$ is only energetically metastable.

B	$B^{\text{numerical}}$	$E^{\text{numerical}}/B$
1	0.9995	93.3151 ± 0.0297
2	1.9994	85.2782 ± 0.0223
3	2.9985	84.0152 ± 0.0200
4	3.9981	83.6919 ± 0.0516
5	4.9959	84.1664 ± 0.0312
6	5.9921	84.7335 ± 0.0204

The boundary conditions for the vortex system are given by

$$f(0) = 0, \quad f(\infty) = \frac{\pi}{2}. \quad (22)$$

We show numerical solutions in Fig. 1 for $m = 1, 4$ and $\kappa = 0, 1$. By the Hopf map, they can (topologically) be mapped to lumps.

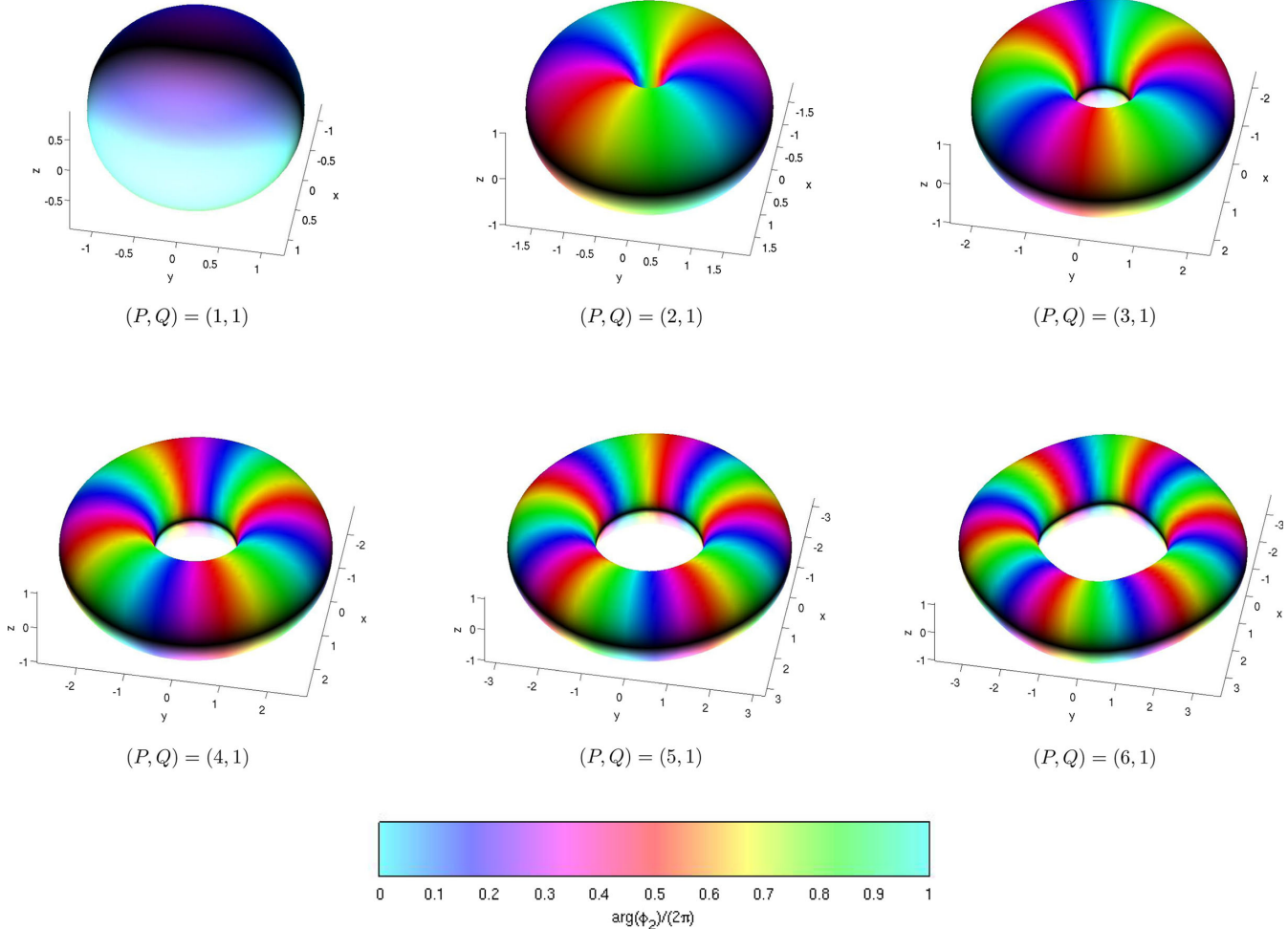


FIG. 6 (color online). Isosurfaces showing the solutions for the $2 + 6$ model, i.e. for $\kappa = 0$ and $c_6 = 1$, at constant baryon charge density equal to half its maximum value. The color represents the phase of the scalar field ϕ_2 , and the lightness is given by $|\Im(\phi_1)|$. The calculations are done on an 81^3 cubic lattice with the relaxation method.

In the final configuration, the U(1) modulus is twisted P times along the toroidal (α) cycle of the torus, and the global string winds Q times “along” the poloidal (β) cycle of the torus; see Fig. 2.

The torus-shaped solution requires us to study the full partial differential equation numerically, for which we

will use the relaxation method on a cubic square lattice. Because of the topological nature of the objects we study, it is sufficient to employ Neumann conditions on the boundary of the lattice whereas the initial condition is very important. For the initial configuration, we will use the Ansatz

$$\phi^T = (\sin [\cos^{-1} \{\sin f(r) \sin \theta\}] e^{i Q \tan^{-1} (\tan f(r) \cos \theta)}, \cos [\cos^{-1} \{\sin f(r) \sin \theta\}] e^{i P \phi}), \quad (24)$$

where $r \in [0, \infty)$, $\theta \in [0, \pi]$, $\varphi \in [0, 2\pi]$ and $f(r)$ is an appropriately chosen monotonically decreasing function satisfying the boundary conditions

$$f(r \rightarrow 0) \rightarrow \pi, \quad f(r \rightarrow \infty) \rightarrow 0. \quad (25)$$

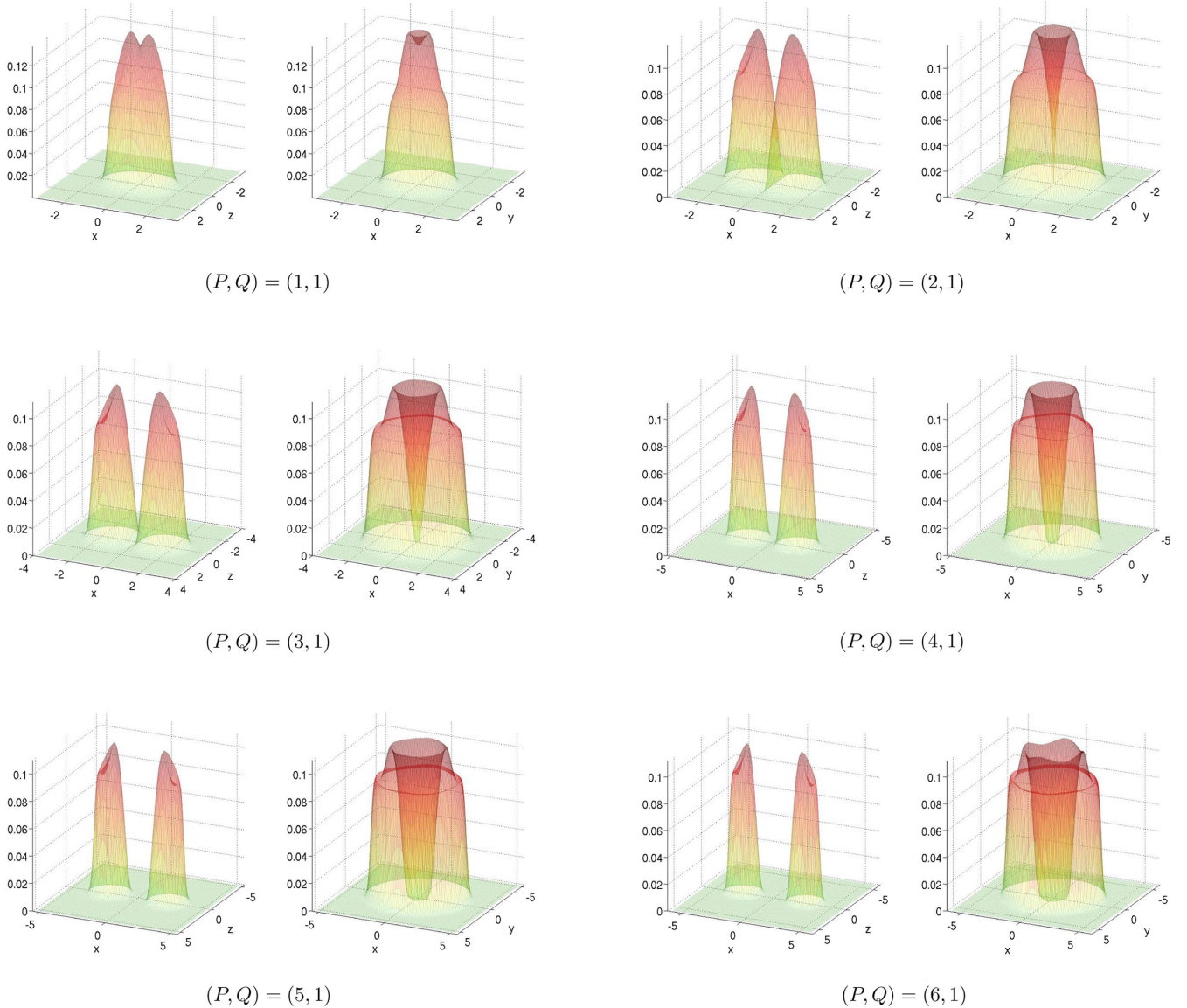
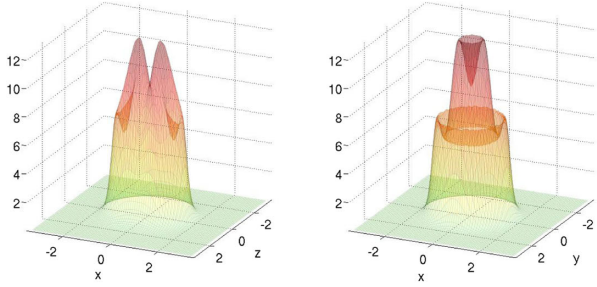


FIG. 7 (color online). Baryon charge density for solutions in the $2 + 6$ model, i.e. with $\kappa = 0$ and $c_6 = 1$, at xz slices (for $y = 0$) and xy slices (for $z = 0$). yz slices are omitted as they are identical to the xz slices by rotational symmetry of the torus. The calculations are done on an 81^3 cubic lattice with the relaxation method.

The baryon number (Skyrme charge) of $\pi_3(S^3) \simeq \mathbb{Z}$ for the configuration given in Eq. (24) is

$$\begin{aligned} B &= \frac{1}{4\pi^2} \int d^3x \epsilon^{ijk} \phi^\dagger \partial_i \phi \partial_j \phi^\dagger \partial_k \phi \\ &= -\frac{1}{2\pi^2} \int_0^\infty dr \int_0^\pi d\theta \int_0^{2\pi} d\phi \sin \theta P Q f'(r) \sin^2 f(r) \\ &= -\frac{PQ}{\pi} \int_0^\infty dr \partial_r [f(r) - \sin f(r) \cos f(r)] \\ &= PQ. \end{aligned} \quad (26)$$

Although we seemingly have two quantum numbers to dial in the configuration, it will prove convenient to think about



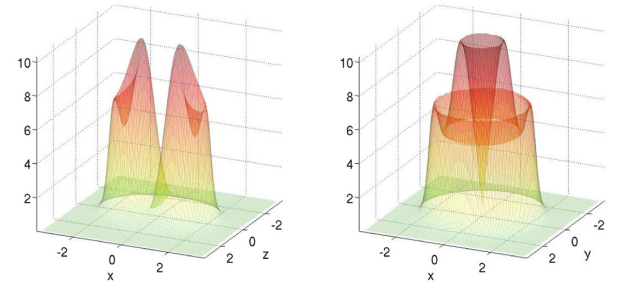
$(P, Q) = (1, 1)$

the winding number Q as that of the global vortex. This may suggest that $Q > 1$ will be unstable as global vortices repel with a force $\sim 1/d$, where d (here) is the separation distance between two strings. We confirm this expectation by numerically solving the equations and we find for $Q > 1$, for a wide range of parameters, that the relaxation method always splits up the object into Q individual strings, each with a P -wound U(1) phase. For details, see Appendix A.

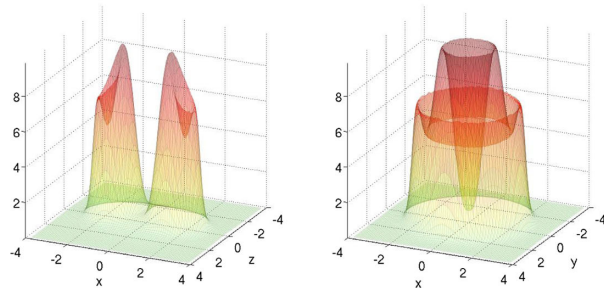
We can therefore study the numerical solutions with baryon number $B = P$, for which the Ansatz (24) reduces to

$$\phi^T = (\cos f(r) + i \sin f(r) \cos \theta, \sin f(r) \sin \theta e^{iP\phi}). \quad (27)$$

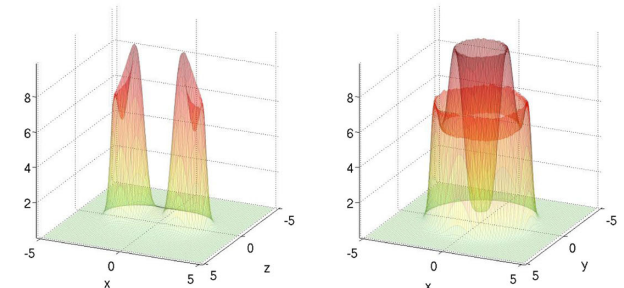
This is exactly the axially symmetric generalization of the hedgehog Ansatz, and this is just what we need (note that for



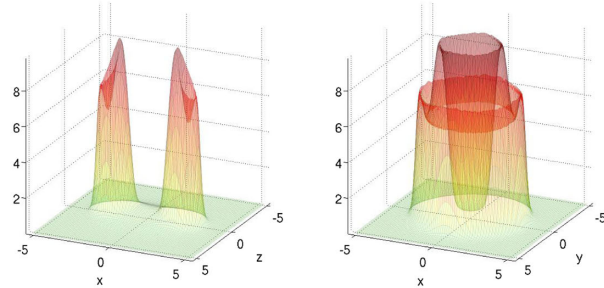
$(P, Q) = (2, 1)$



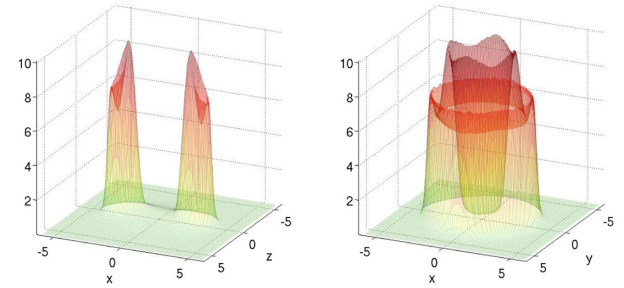
$(P, Q) = (3, 1)$



$(P, Q) = (4, 1)$



$(P, Q) = (5, 1)$



$(P, Q) = (6, 1)$

FIG. 8 (color online). Energy density for solutions in the $2 + 6$ model, i.e. with $\kappa = 0$ and $c_6 = 1$, at xz slices (for $y = 0$) and xy slices (for $z = 0$). yz slices are omitted as they are identical to the xz slices by rotational symmetry of the torus. The calculations are done on an 81^3 cubic lattice with the relaxation method.

TABLE II. Numerically integrated baryon charge and energy (mass) for the solutions in the $2 + 6$ model. Stability is observed for the first five solutions, while $P = 6$ is only energetically metastable.

B	$B^{\text{numerical}}$	$E^{\text{numerical}} / B$
1	0.9999	100.8613 ± 0.0410
2	1.9998	89.7184 ± 0.0532
3	2.9995	87.3095 ± 0.1871
4	3.9981	87.5179 ± 0.0721
5	4.9970	87.5560 ± 0.0901
6	5.9939	88.1414 ± 0.1145

Skyrmions without our BEC-motivated potential, this Ansatz is only appropriate for $B = 1, 2$ while for $B > 2$ the axial symmetry no longer yields the minimum-energy configuration). We will study two cases in turn: in the first we turn on only the fourth-order derivative term, i.e. $\kappa = 1$ and $c_6 = 0$, while in the second case, we switch off the fourth-order but use the sixth-order derivative term, i.e. $\kappa = 0$ and $c_6 = 1$. We will call them the $2 + 4$ model and the $2 + 6$ model, respectively.

In Figs. 3, 4, and 5, we show solutions for case of the $2 + 4$ model ($\kappa = 1$ and $c_6 = 0$) with mass $m = 4$. In Fig. 3 is shown the three-dimensional isosurfaces at half the

maximum value of the baryon charge density. The color scheme used is chosen such that the U(1) phase, $\arg\phi_2$, is mapped to the hue while the lightness is given by the absolute value of the imaginary part of the vortex condensate: $|\Im(\phi_1)|$. In Figs. 4 and 5 are shown the baryon charge density and energy density, at two different cross sections cutting through the origin of the torus, respectively. In this case, they are practically identical, which means that the energy density is located where the baryon charge is.

As a check on our numerical precision, we calculate the baryon charge density and integrate it numerically; see Table I. As already explained, our Skyrmionic torii are only stable for $Q = 1$, but to study whether they are stable for higher $P > 1$, we need to compare the energy of the configurations. In Table I we calculate the energy per $B = P$ and find that the energy drops for the first four torii, viz. $P = 1, 2, 3, 4$, but then it starts to increase slightly. The increase is so small that the $P = 5$ solution is still energetically stable (also taking into account the numerical accuracy) while $P = 6$ is only metastable [30]. That is, the energy of the $P = 6$ solution is larger than two times that of the $P = 3$ solution, and hence it is bound to decay. Here we have not studied the potential barrier for the decay and thus cannot calculate its lifetime.

Next we will turn to the case of the $2 + 6$ model, i.e. with only sixth-order derivative terms ($\kappa = 0$ and $c_6 = 1$) and

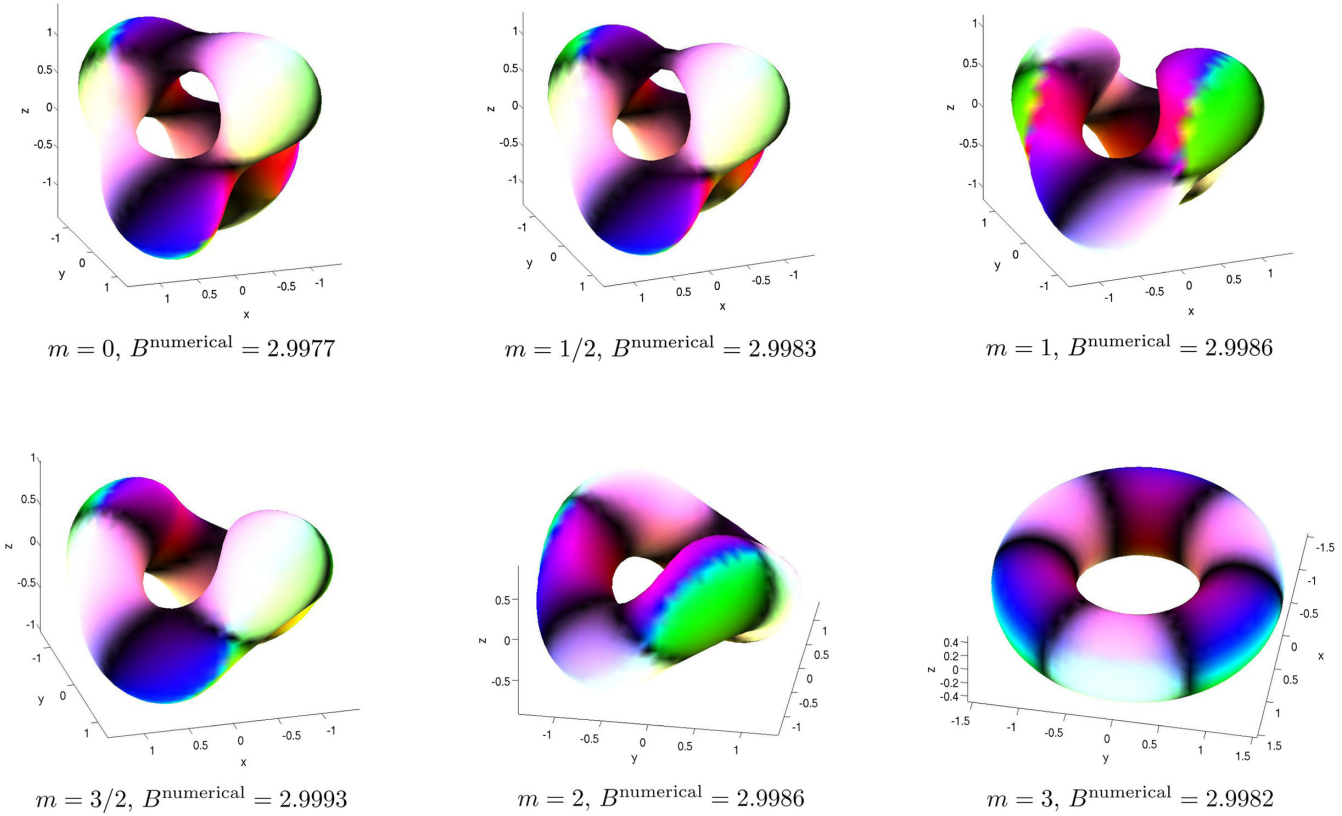


FIG. 9 (color online). Isosurfaces showing the solutions for the $2 + 4$ model, $B = 3$ and various values of the mass parameter, m , and the tetrahedral Ansatz (29) as the initial guess for the relaxation. The color represents the phase of the scalar field ϕ_2 , and the lightness is given by $|\Im(\phi_1)|$. The calculations are done on an 81^3 cubic lattice with the relaxation method.

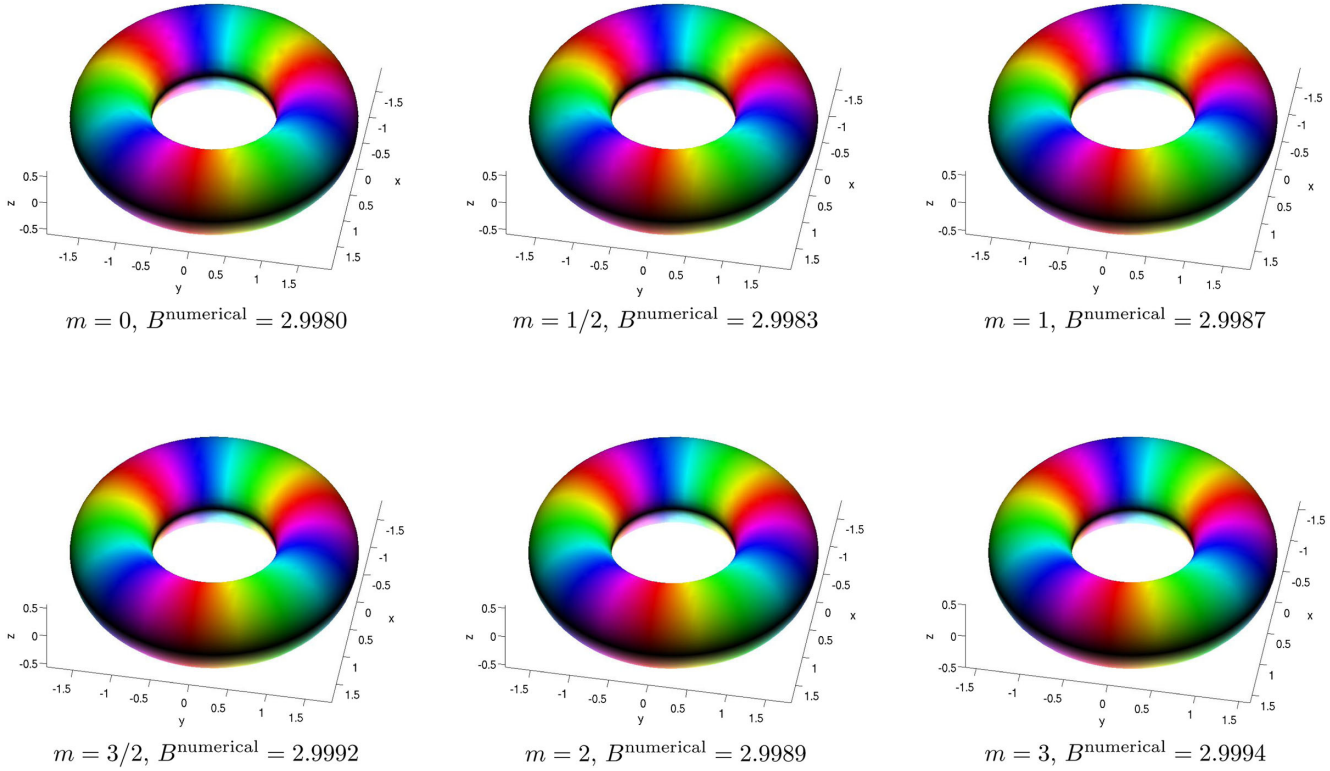


FIG. 10 (color online). Isosurfaces showing the solutions for the $2 + 4$ model, $B = 3$ and various values of the mass parameter, m , and the toroidal Ansatz (27) as the initial guess for the relaxation. The color represents the phase of the scalar field ϕ_2 , and the lightness is given by $|\Im(\phi_1)|$. The calculations are done on an 81^3 cubic lattice with the relaxation method.

again with a mass of $m = 4$. Numerical solutions are shown in Figs. 6, 7, and 8. As in the previous case, we show the three-dimensional isosurfaces of the baryon charge density at half the maximum value in Fig. 6. In Figs. 7 and 8 are shown the baryon charge density and energy density, respectively, at two different cross sections cutting the torus through the origin. Notice that the energy densities for these solutions are somewhat more complex than their respective baryon charge densities. This is one difference between the $2 + 6$ model and the $2 + 4$ model. The second difference is that in this case the torus shape is vaguely visible already for $P = 1$, whereas for the previous case, $P = 1$ has (unbroken) spherical symmetry. Let us also comment on the circular shape of the torus for the $(P, Q) = (6, 1)$ solution along the toroidal direction in Fig. 6; this flattening out of the circle is not aligned with the lattice but is at almost 45° to the lattice axis. Since the small P solutions do possess almost perfect circular symmetry, we believe that this is not a lattice effect but instead signals metastability of the string; for high enough $B = P$, the string wants to collapse and break up. The same effect can also be observed in the $(P, Q) = (6, 1)$ solution in Fig. 8 on the xy slice where the energy density displays four distinct wave tops around the toroidal cycle.

We again check the numerical precision by numerically evaluating the total baryon charge; see Table II. As for the stability of the higher $P > 1$ solutions, we numerically

evaluate the energy (mass) of the solutions and again find that the energy decreases as P is increased, for the first few solutions, but this time only for the first three $P = 1, 2, 3$, and then it starts to increase slightly. The first

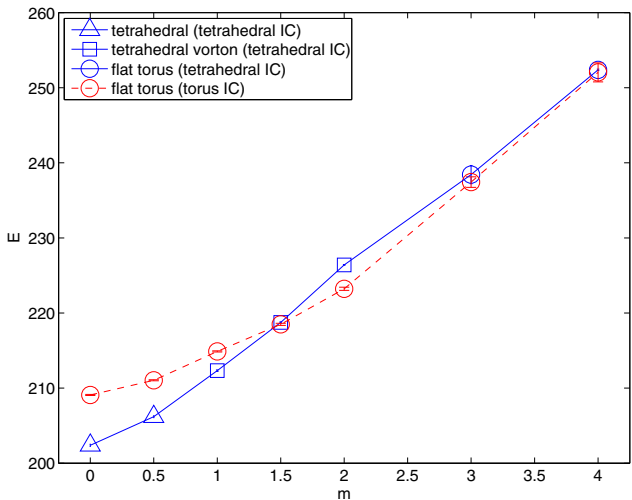


FIG. 11 (color online). Energies of numerical solutions of which the initial guesses are tetrahedrals (blue line) and torii (red line) with varying mass m . For small $m \leq 1$ the tetrahedral Ansatz gives tetrahedral solutions. At $m \gtrsim 1.5$ the tetrahedral Ansatz gives rise to solutions that are heavier than that with the toroidal Ansatz, suggesting a first-order phase transition. For large $m \gtrsim 3$ both series give torii.

five solutions are all energetically *stable*, while $P = 6$ is only metastable.

V. TRANSITION TO TOROIDAL SKYRMIONS

In this section we study the transition from the normal Skyrmion of higher charge (i.e. with $m = 0$) to the toroidal Skyrmion (i.e. with m sufficiently large). For concreteness we study the transition in the normal Skyrme model ($\kappa = 1$ and $c_6 = 0$) and for $B = 3$ where the transition is very visible (as opposed to for instance $B = 1$ and $B = 2$). When the potential is turned off, the $B = 3$ Skyrmion in the normal Skyrme model is of tetrahedral shape [31]. Turning on the potential (9), vortonlike Skyrmions become the lowest-energy state for a sufficiently large mass parameter, m . To find the critical mass necessary for obtaining torii or global strings in the Skyrme model, we vary the mass parameter and repeat the numerical calculation. We are using the relaxation method to find numerical solutions. One weakness of this method is that it only finds the nearest *local* minimal-energy solution, as opposed to the *global* one. For this reason we make two series of numerical

calculations. One starts from the tetrahedral solution, of which the initial guess is [32]

$$\mathbf{n} = \left\{ \frac{R + \bar{R}}{1 + R\bar{R}} \sin f, \frac{i(\bar{R} - R)}{1 + R\bar{R}} \sin f, \frac{1 - R\bar{R}}{1 + R\bar{R}} \sin f, \cos f \right\}, \quad (28)$$

where R is the rational map Ansatz and for $B = 3$ the tetrahedral Ansatz is [32]

$$R = \frac{z^3 - \sqrt{3}iz}{\sqrt{3}iz^2 - 1}, \quad z = \tan\left(\frac{\theta}{2}\right)e^{i\phi}, \quad (29)$$

where θ, ϕ are angles on the 2-sphere. The other series of numerical solutions uses the initial guess provided by the torus Ansatz of Eq. (27).

Figures 9 and 10 show the two series of numerical solutions starting from the tetrahedral and toroidal initial guess, respectively. It is observed that for $m \gtrsim 3$ both series converge to a flat torus. The difference in the colors is due to a permutation in the fields n_3 and n_2 . The two flat torii

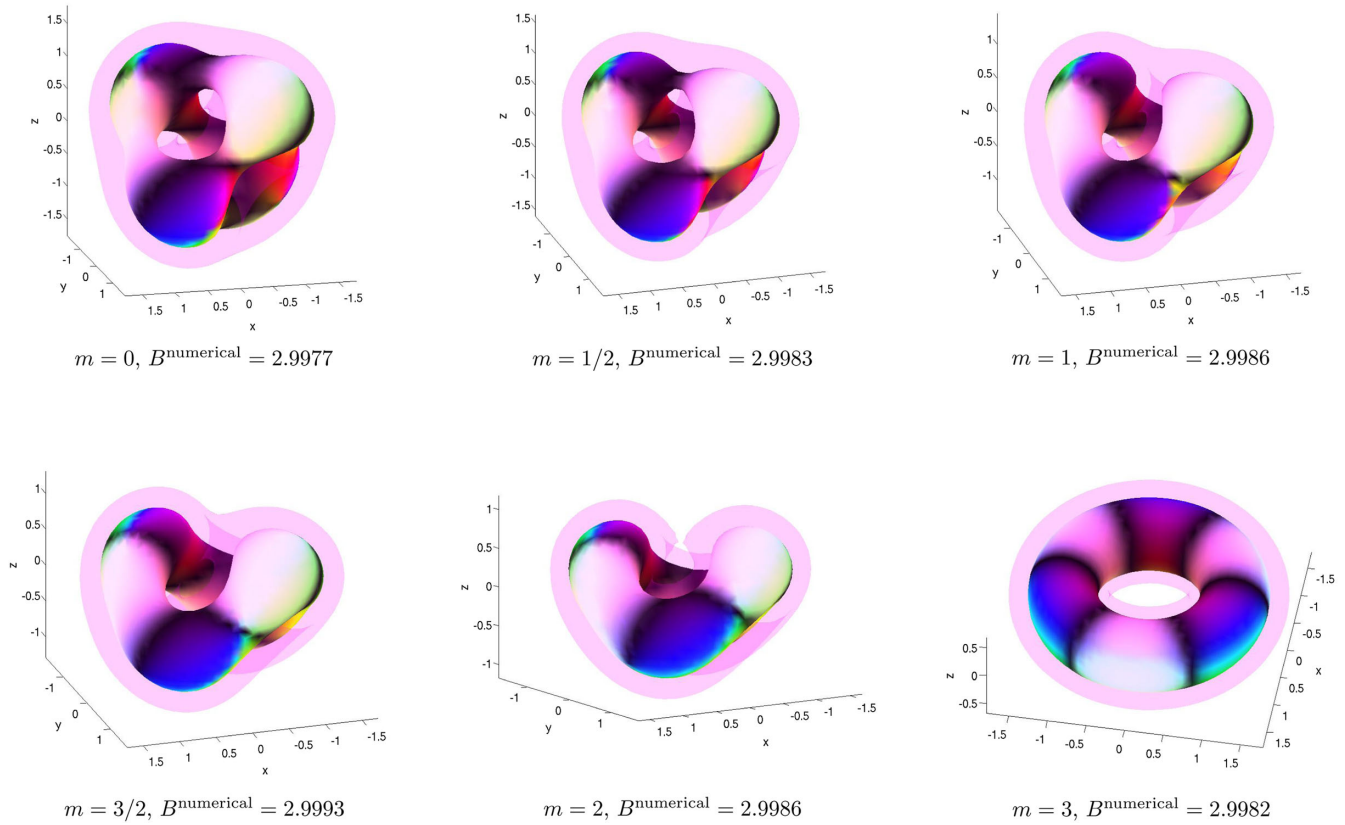


FIG. 12 (color online). Isosurfaces showing the solutions for the $2 + 4$ model, for $B = 3$ and various values of the mass parameter, m , and the tetrahedral Ansatz (29) as the initial guess for the relaxation. The colored isosurface and the magenta shadow show the isosurface at half and a quarter of the maximal value of the baryon charge density, respectively. The color represents the phase of the scalar field ϕ_2 , and the lightness is given by $|\Im(\phi_1)|$. The calculations are done on an 81^3 cubic lattice with the relaxation method.

for $m = 4$ are physically the same and are not shown in Figs. 9 and 10, but can be seen in Fig. 3.

To determine which state is the lowest-energy state, we also compare the energies for the two series of numerical solutions. In Fig. 11 we show the energies of the two series of numerical solutions: the blue solid line shows the solution of which the initial guess is the tetrahedral Ansatz, and the red dashed line has the torus Ansatz as the initial guess. We see that for $m \lesssim 1.5$ the tetrahedral is the lowest-energy state. Our calculation indicates that a first-order phase transition takes place around $m = m_{\text{critical}} \sim 1.5$, where the tetrahedral state rises above that of the toroidal one. For $m \gtrsim 3$ both Ansätze give a flat torus after relaxation has found a solution. Thus, the tetrahedral state either becomes unstable or slowly merges together with that of the toroidal one. The instability sets in for m between 3 and 4. To check that the phase transition around $m \sim 1.5$ really takes place, we have run the solutions with an exceptionally long relaxation time and found solutions with a very high accuracy (the equations of motion are satisfied at every spatial position better than 10^{-4} and about 10^{-5} on average). Indicative of the two different states crossing around the critical mass, $m_{\text{critical}} \sim 1.5$, is that the two different solutions have almost exactly the same energy.

To see that the numerical solutions for m between 1 and 2 are actually tetrahedral in nature as opposed to bent torii, we show the solutions with colored isosurfaces at half the maximal value as well as at a quarter of the maximal value of the baryon charge density in Fig. 12. It is observed that there is a cloud connecting the solution between the string at antipodal points. For sufficiently large $m \sim 2m_{\text{critical}}$, the tetrahedral solution becomes unstable, and thus for large m only the torus exists.

VI. SUMMARY AND DISCUSSION

We have studied Skyrmion solutions in the BEC Skyrme model, which is a Skyrme model with the potential term motivated by two-component BECs. We have constructed stable Skyrmion solutions for $P = 1, 2, 3, 4, 5$ and $Q = 1$, yielding the baryon numbers $B = 1, 2, 3, 4, 5$ as well as a metastable solution for $P = 6$ and $Q = 1$ ($B = 6$). We suspect that higher baryon charged solutions will all be metastable. The energy and baryon charge distributions of the configurations with $P > 1$ are all of toroidal shape. They are vortex rings of the field ϕ_1 , with the field ϕ_2 trapped in their cores, where the phase of the field ϕ_2 winds P times along the ring. We have found that configurations with charge (P, Q) decay into Q rings of charge $(P, 1)$. This string splitting can be understood as the repulsion of global vortex strings. Finally we have discovered a first-order phase transition between Skyrmions with a discrete point symmetry and axial (toroidal) symmetry.

In two-component BECs, one can introduce a Rabi oscillation term $\gamma(\phi_1(x)^*\phi_2(x) + \text{c.c.})$, known as a Josephson term in superconductors, in the Lagrangian. Introduction of this term deforms the Skyrmions inside a domain wall [25,28,33,34]. What deformation this term introduces for toroidal Skyrmions in the BEC Skyrme model remains as a future problem. On the other hand, if we introduce the potential term $V \sim \phi_1 + \phi_1^*$ [17], our configurations will become P sine-Gordon kinks on a vortex ring, which is a $(3 + 1)$ -dimensional analog of Ref. [35], in which sine-Gordon kinks on a domain wall ring were constructed in $2 + 1$ dimensions.

Two-component BECs are known to admit a stable composite soliton, viz. a D-brane soliton, that is, a domain wall on which vortices end from both sides [36], originally found in the massive \mathbb{CP}^1 model [37,38]. The (BEC) Skyrme model discussed in this paper has the same potential term and is expected to admit such a D-brane soliton. A configuration made of a domain wall and an anti-domain wall stretched by lump strings in the massive \mathbb{CP}^1 model was considered in Ref. [39], in which it was discussed that such a configuration is unstable to decay, resulting in the creation of Hopfions. Therefore, the same mechanism should work also in the (BEC) Skyrme model discussed in this paper creating Skyrmions from brane annihilation, as was discussed for two-component BECs [8].

The Bogomol'nyi–Prasad–Sommerfield Skyrme model, proposed recently [19], consists of only the sixth-order derivative term as well as appropriate potentials. This model admits exact solutions with compact support. By choosing the potential of the BEC Skyrme model in this paper, we may be able to construct exact solutions of Skyrmions with toroidal shape.

The Skyrmions with the charge (P, Q) are related through the Hopf map to (P, Q) Hopfions [40,41] in the Ising Faddeev–Skyrme (FS) model [39], that is, the FS model [42,43] with an Ising-type potential term admitting two discrete vacua. The domain wall in the BEC Skyrme model is mapped to a domain wall with a U(1) modulus interpolating between these two vacua [23,24,27], and a global vortex is mapped to a lump or baby Skyrmiion [44,45]. This model also admits a twisted domain-wall tube with the U(1) modulus twisted along the cycle of the tube [35] as a baby-Skyrmiion string. The original FS model without said potential term is known to admit Hopfions, i.e. solitons with Hopf charge $\pi_3(S^2) \simeq \mathbb{Z}$ [15,43,46–50], and, in particular, Hopfions with Hopf charge 7 or higher were found to have knot structures [48–50]. The (P, Q) Hopfions in the Ising FS model are not knots but toroidal domain walls characterized by two integers (P, Q) , where the U(1) modulus of the domain wall is twisted P and Q times along the toroidal and poloidal cycles of the torus, respectively. In this case, some configurations with $Q > 1$ were found to be stable [41],

unlike our case of Skyrmions for which all configurations for $Q > 1$ are unstable. This is because there is no repulsion between lumps.

If we consider compactifying space to $\mathbb{R}^2 \times S^1$, we have another solution in addition to the one studied here, in which the vortex string extends along the S^1 direction and has P twists on its U(1) modulus. The corresponding solution for the case of the Hopfion was discussed in Ref. [51]. Skyrmions in the conventional model on $S^2 \times S^1$ were discussed in Ref. [52].

ACKNOWLEDGMENTS

We thank Michikazu Kobayashi for discussions in the early stage of this work. The work of M. N. is supported in part by Grant-in-Aid for Scientific Research, Grant

No. 25400268, and by the “Topological Quantum Phenomena” Grant-in-Aid for Scientific Research on Innovative Areas (Grant No. 25103720) from the Ministry of Education, Culture, Sports, Science and Technology (MEXT) of Japan. S. B. G. thanks Keio University for hospitality during which this project took shape. The authors thank the referee for valuable comments.

APPENDIX A: STRING SPLITTING FOR $Q > 1$

In this section we show that the relaxation of the $(P, Q) = (P, 2)$ torus splits into two separate $(P, Q) = (P, 1)$ objects for $P = 1, 2$. For concreteness we carry out the calculations in the 2 + 6 model ($\kappa = 0$ and $c_6 = 1$). In Figs. 13 and 14 are shown the $(1, 2) \rightarrow 2 \times (1, 1)$ and

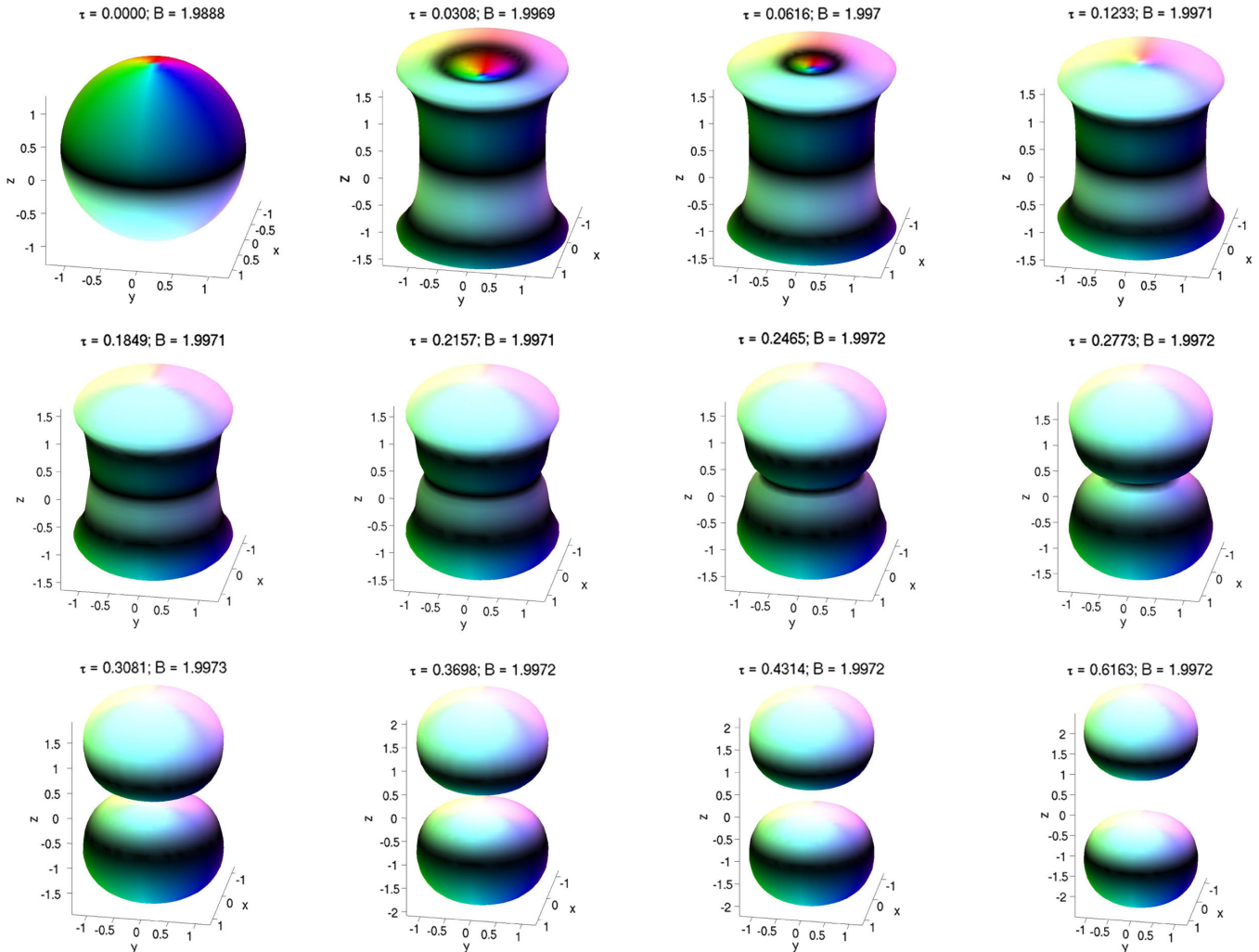


FIG. 13 (color online). Isosurfaces showing an initial configuration with $(P, Q) = (1, 2)$ ($B = 2$) in 2 + 6 model ($\kappa = 0$, $c_6 = 1$ and $m = 4$) which after some finite relaxation time splits the Skyrmion into two separate Skyrmions of charge 1, i.e. $(P, Q) = (1, 1)$. The isosurfaces show constant baryon charge density equal to half its maximum value. The color represents the phase of the scalar field ϕ_2 , and the lightness is given by $|\Im(\phi_1)|$. The calculation is carried out on an 81^3 cubic lattice with the relaxation method.

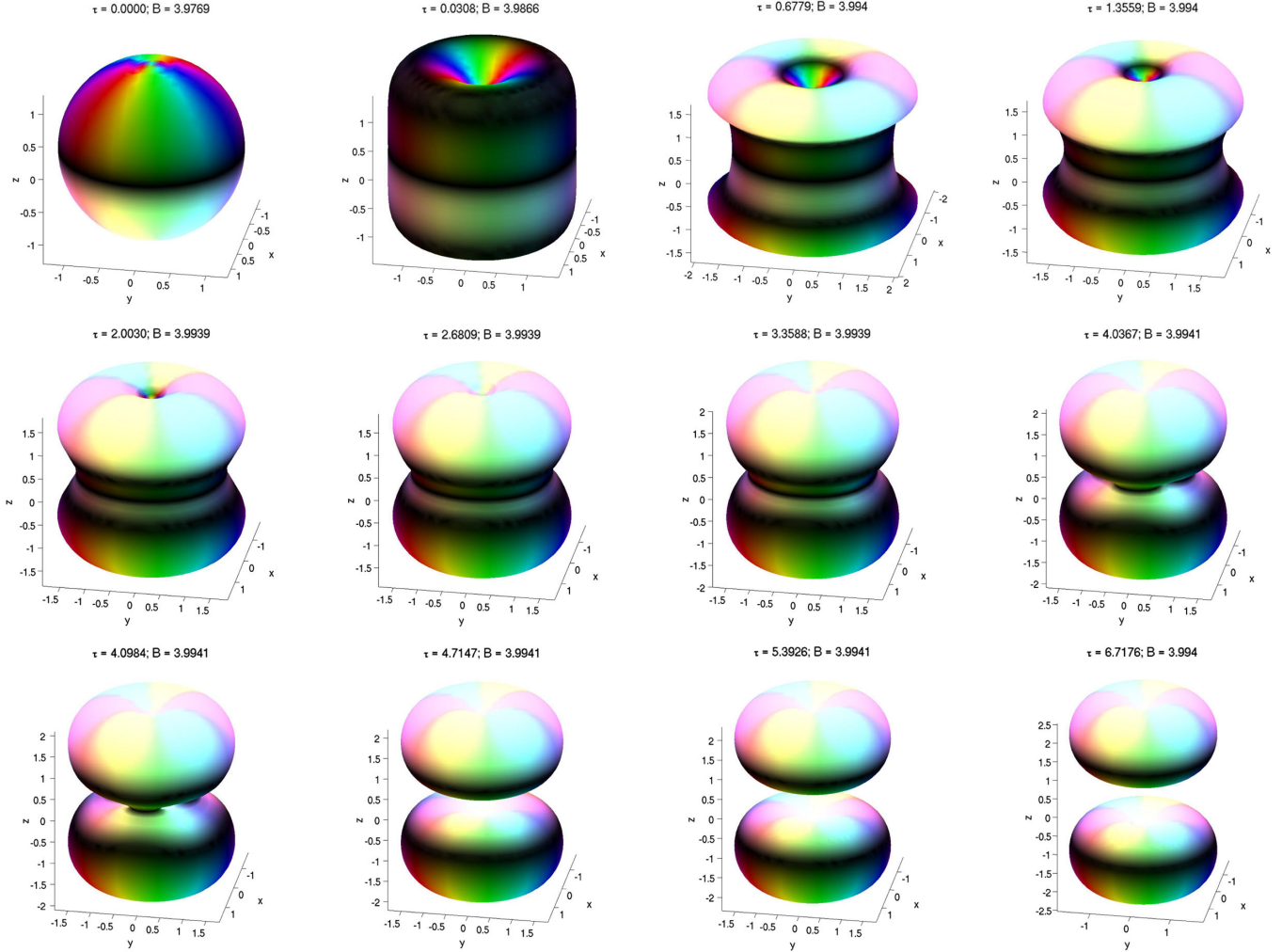


FIG. 14 (color online). Isosurfaces showing an initial configuration with $(P, Q) = (2, 2)$ ($B = 4$) in the $2 + 6$ model ($\kappa = 0$, $c_6 = 1$ and $m = 4$) which after some finite relaxation time splits the Skyrmion into two separate Skyrmions of charge 2, i.e. $(P, Q) = (2, 1)$. The isosurfaces show constant baryon charge density equal to half its maximum value. The color represents the phase of the scalar field ϕ_2 , and the lightness is given by $|\Im(\phi_1)|$. The calculation is carried out on an 81^3 cubic lattice with the relaxation method.

$(2, 2) \rightarrow 2 \times (2, 1)$ string splittings as function of relaxation time τ , respectively.

APPENDIX B: COMPARISON OF TORUS AND SKYRMION

In this section we will compare the case of $(P, Q) = (2, 1)$ and thus baryon number 2 and $m = 4$, where the Skyrmion is a torus, with the case of $m = 0$, which is just the normal $B = 2$ Skyrmion and also in the form of a torus. We will make the comparison for

both the $2 + 4$ model and the $2 + 6$ model. In Figs. 15 and 16 are shown the comparison for the $2 + 4$ and $2 + 6$ models, respectively. For the $2 + 4$ model, the main difference is the size (and in turn the total mass) of the two solutions. For the $2 + 6$ model, differences are evident both in the baryon charge density slices (middle row) and the energy density slices (bottom row). For the BEC Skyrmion in the $2 + 6$ model, the torus is more hollow with respect to its potential-less counterpart.

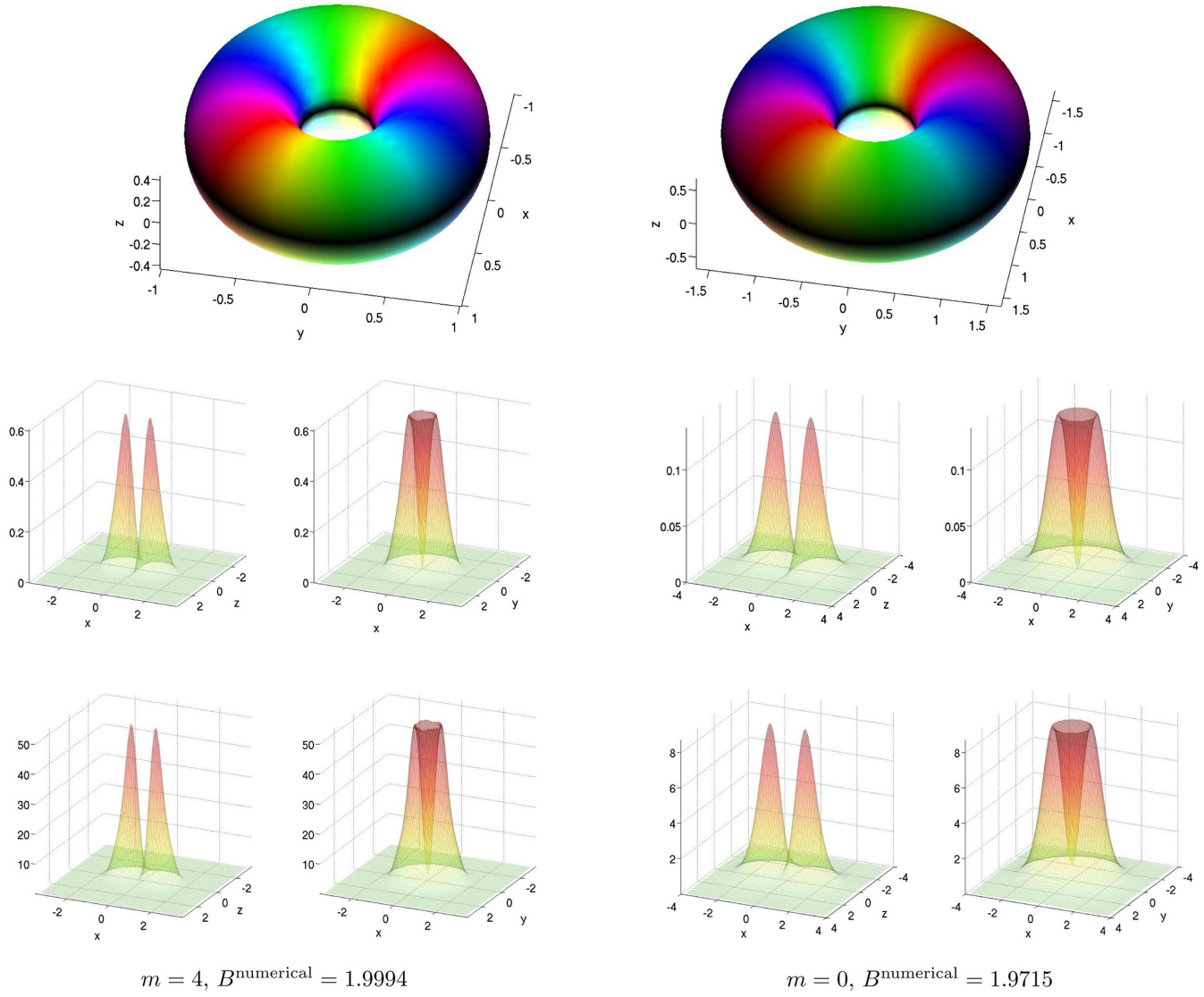


FIG. 15 (color online). Comparison between the BEC Skyrmiion in the $2 + 4$ model ($m = 4$) on the left and the normal Skyrmiion ($m = 0$) on the right. From top to bottom is shown the isosurface of the baryon density at half maximum, the baryon density at xz and xy slices through the origin of the torus, and finally similar energy density slices.

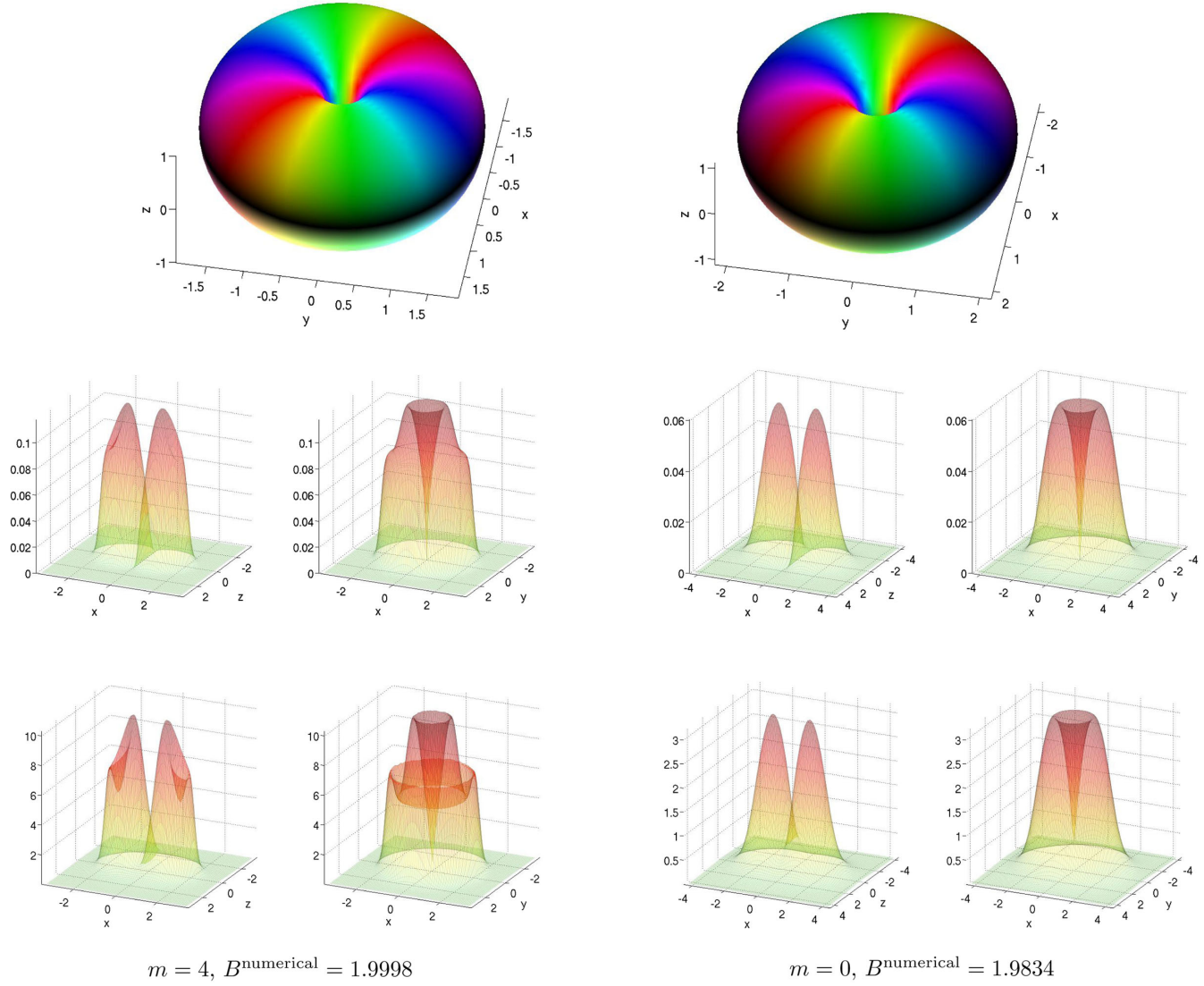


FIG. 16 (color online). Comparison between the BEC Skyrmiion in the $2 + 6$ model ($m = 4$) on the left and the “normal” Skyrmiion in the $2 + 6$ model ($m = 0$) on the right. From top to bottom is shown the isosurface of the baryon density at half maximum, the baryon density at xz and xy slices through the origin of the torus, and finally similar energy density slices.

- [1] T. H. R. Skyrme, A unified field theory of mesons and baryons, *Nucl. Phys.* **31**, 556 (1962); A nonlinear field theory, *Proc. R. Soc. A* **260**, 127 (1961).
- [2] G. S. Adkins, C. R. Nappi, and E. Witten, Static properties of nucleons in the Skyrme model, *Nucl. Phys.* **B228**, 552 (1983).
- [3] T. Sakai and S. Sugimoto, Low energy hadron physics in holographic QCD, *Prog. Theor. Phys.* **113**, 843 (2005); More on a holographic dual of QCD, *Prog. Theor. Phys.* **114**, 1083 (2005).
- [4] H. Hata, T. Sakai, S. Sugimoto, and S. Yamato, Baryons from instantons in holographic QCD, *Prog. Theor. Phys.* **117**, 1157 (2007).

- [5] J. Ruostekoski and J. R. Anglin, Creating Vortex Rings and Three-Dimensional Skyrmions in Bose-Einstein Condensates, *Phys. Rev. Lett.* **86**, 3934 (2001); R. A. Battye, N. R. Cooper, and P. M. Sutcliffe, Stable Skyrmions in Two-Component Bose-Einstein Condensates, *Phys. Rev. Lett.* **88**, 080401 (2002).
- [6] U. A. Khawaja and H. T. C. Stoof, Skyrmions in a ferromagnetic Bose-Einstein condensate, *Nature (London)* **411**, 918 (2001); Skyrmion Physics in Bose-Einstein Ferromagnets, *Phys. Rev. A* **64**, 043612 (2001); C. M. Savage and J. Ruostekoski, Energetically Stable Particle-Like Skyrmions in a Trapped Bose-Einstein Condensate, *Phys. Rev. Lett.* **91**,

- 010403 (2003); J. Ruostekoski, Stable Particlelike Solitons with Multiply-Quantized Vortex Lines in Bose-Einstein Condensates, *Phys. Rev. A* **70**, 041601 (2004); S. Wuster, T. E. Argue, and C. M. Savage, Numerical Study of the Stability of Skyrmions in Bose-Einstein Condensates, *Phys. Rev. A* **72**, 043616 (2005); I. F. Herbut and M. Oshikawa, Stable Skyrmions in Spinor Condensates, *Phys. Rev. Lett.* **97**, 080403 (2006); A. Tokuno, Y. Mitamura, M. Oshikawa, and I. F. Herbut, Skyrmion in Spinor Condensates and its Stability in Trap Potentials, *Phys. Rev. A* **79**, 053626 (2009).
- [7] T. Kawakami, T. Mizushima, M. Nitta, and K. Machida, Stable Skyrmions in SU(2) Gauged Bose-Einstein Condensates, *Phys. Rev. Lett.* **109**, 015301 (2012).
- [8] M. Nitta, K. Kasamatsu, M. Tsubota, and H. Takeuchi, Creating Vortons and Three-Dimensional Skyrmions from Domain Wall Annihilation with Stretched Vortices in Bose-Einstein Condensates, *Phys. Rev. A* **85**, 053639 (2012).
- [9] K. Kasamatsu, M. Tsubota, and M. Ueda, Vortices in multicomponent Bose-Einstein condensates, *Int. J. Mod. Phys. B* **19**, 1835 (2005).
- [10] H. Takeuchi, K. Kasamatsu, M. Tsubota, and M. Nitta, Tachyon Condensation Due to Domain-Wall Annihilation in Bose-Einstein Condensates, *Phys. Rev. Lett.* **109**, 245301 (2012); H. Takeuchi, K. Kasamatsu, M. Nitta, and M. Tsubota, Vortex formations from domain wall annihilations in two-component Bose-Einstein condensates, *J. Low Temp. Phys.* **162**, 243 (2011); H. Takeuchi, K. Kasamatsu, M. Tsubota, and M. Nitta, Tachyon condensation and brane annihilation in Bose-Einstein condensates: Spontaneous symmetry breaking in restricted lower-dimensional subspace, *J. Low Temp. Phys.* **171**, 443 (2013).
- [11] It has also been proposed that a stable three-dimensional Skyrmion can exist as a ground state in the SU(2)-symmetric case, by introducing “artificial” non-Abelian gauge fields [7].
- [12] M. A. Metlitski and A. R. Zhitnitsky, Vortex rings in two-component Bose-Einstein condensates, *J. High Energy Phys.* **06** (2004) 017.
- [13] R. L. Davis and E. P. S. Shellard, The physics of vortex superconductivity. 2, *Phys. Lett. B* **209**, 485 (1988); “Cosmic vortons”, *Nucl. Phys.* **B323**, 209 (1989).
- [14] A. Vilenkin and E. P. S. Shellard, *Cosmic Strings and Other Topological Defects*, Cambridge Monographs on Mathematical Physics (Cambridge University Press, Cambridge, England, 2000).
- [15] E. Radu and M. S. Volkov, Stationary ring solitons in field theory—Knots and vortons, *Phys. Rept.* **468**, 101 (2008).
- [16] J. Garaud, E. Radu, and M. S. Volkov, Stable Cosmic Vortons, *Phys. Rev. Lett.* **111**, 171602 (2013).
- [17] S. B. Gudnason and M. Nitta, Incarnations of Skyrmions, *Phys. Rev. D* **90**, 085007 (2014).
- [18] S. B. Gudnason and M. Nitta, Effective field theories on solitons of generic shapes, *arXiv:1407.2822*.
- [19] C. Adam, J. Sanchez-Guillen, and A. Wereszczynski, A Skyrme-type proposal for baryonic matter, *Phys. Lett. B* **691**, 105 (2010); A BPS Skyrme Model and Baryons at Large N_c , *Phys. Rev. D* **82**, 085015 (2010).
- [20] S. B. Gudnason and M. Nitta, Baryonic Sphere: A Spherical Domain Wall Carrying Baryon Number, *Phys. Rev. D* **89**, 025012 (2014).
- [21] Strictly speaking, there is a supercurrent or a superflow due to the trapped field along the ring of the vorton. This can be achieved by rotating the phase of the trapped field linearly in time as $\phi_2 \sim e^{iz+iat}$ with z being the coordinate along the string. In the case of BECs, such a time dependence is automatic in the presence of the phase gradient along the string because of the first derivative in time in the non-relativistic Lagrangian.
- [22] M. Kobayashi and M. Nitta, Non-Relativistic Nambu-Goldstone Modes Associated with Spontaneously Broken Space-Time and Internal Symmetries, *Phys. Rev. Lett.* **113**, 120403 (2014).
- [23] E. R. C. Abraham and P. K. Townsend, Q kinks, *Phys. Lett. B* **291**, 85 (1992); More on Q kinks: A (1 + 1)-dimensional analog of dyons, *Phys. Lett. B* **295**, 225 (1992).
- [24] M. Arai, M. Naganuma, M. Nitta, and N. Sakai, Manifest supersymmetry for BPS walls in $N = 2$ nonlinear sigma models, *Nucl. Phys.* **B652**, 35 (2003); *A Garden of Quanta*, edited by (World Scientific, Singapore, 2003).
- [25] M. Nitta, Josephson Vortices and the Atiyah-Manton Construction, *Phys. Rev. D* **86**, 125004 (2012).
- [26] M. Nitta, Defect Formation from Defect-Anti-Defect Annihilations, *Phys. Rev. D* **85**, 101702 (2012).
- [27] A. E. Kudryavtsev, B. M. A. Piette, and W. J. Zakrzewski, Skyrmions and domain walls in (2 + 1) dimensions, *Nonlinearity* **11**, 783 (1998); D. Harland and R. S. Ward, Walls and Chains of Planar Skyrmions, *Phys. Rev. D* **77**, 045009 (2008).
- [28] M. Nitta, Correspondence between Skyrmions in 2 + 1 and 3 + 1 Dimensions, *Phys. Rev. D* **87**, 025013 (2013); Matryoshka skyrmions, *Nucl. Phys.* **B872**, 62 (2013).
- [29] E. Witten, Superconducting strings, *Nucl. Phys.* **B249**, 557 (1985).
- [30] The question of stability may also depend on the coefficients of the higher-derivative terms and the mass.
- [31] R. A. Battye and P. M. Sutcliffe, Symmetric Skyrmions, *Phys. Rev. Lett.* **79**, 363 (1997).
- [32] C. J. Houghton, N. S. Manton, and P. M. Sutcliffe, Rational maps, monopoles and Skyrmions, *Nucl. Phys.* **B510**, 507 (1998).
- [33] S. B. Gudnason and M. Nitta, Domain Wall Skyrmions, *Phys. Rev. D* **89**, 085022 (2014).
- [34] J. Garaud and E. Babaev, Skyrmionic state and stable half-quantum vortices in chiral p-wave superconductors, *Phys. Rev. B* **86**, 060514 (2012).
- [35] M. Kobayashi and M. Nitta, Sine-Gordon kinks on a domain wall ring, *Phys. Rev. D* **87**, 085003 (2013).
- [36] K. Kasamatsu, H. Takeuchi, M. Nitta, and M. Tsubota, Analogues of D-branes in Bose-Einstein condensates, *J. High Energy Phys.* **11** (2010) 068; K. Kasamatsu, H. Takeuchi, and M. Nitta, D-brane solitons and boojums in field theory and Bose-Einstein condensates, *J. Phys. Condens. Matter* **25**, 404213 (2013); K. Kasamatsu, H. Takeuchi, M. Tsubota, and M. Nitta, Wall-Vortex Composite Solitons in Two-Component Bose-Einstein Condensates, *Phys. Rev. A* **88**, 013620 (2013).

- [37] J. P. Gauntlett, R. Portugues, D. Tong, and P. K. Townsend, D-Brane Solitons in Supersymmetric Sigma Models, *Phys. Rev. D* **63**, 085002 (2001); M. Shifman and A. Yung, Domain Walls and Flux Tubes in $N = 2$ SQCD: D-Brane Prototypes, *Phys. Rev. D* **67**, 125007 (2003).
- [38] Y. Isozumi, M. Nitta, K. Ohashi, and N. Sakai, All Exact Solutions of a 1/4 Bogomol'nyi-Prasad-Sommerfield Equation, *Phys. Rev. D* **71**, 065018 (2005); M. Eto, Y. Isozumi, M. Nitta, K. Ohashi, and N. Sakai, Solitons in the Higgs phase: The Moduli matrix approach, *J. Phys. A* **39**, R315 (2006); M. Eto, Y. Isozumi, M. Nitta, and K. Ohashi, 1/2, 1/4 and 1/8 BPS equations in SUSY Yang-Mills-Higgs systems: Field theoretical brane configurations, *Nucl. Phys. B* **752**, 140 (2006).
- [39] M. Nitta, Knots from Wall-Anti-Wall Annihilations with Stretched Strings, *Phys. Rev. D* **85**, 121701 (2012).
- [40] M. Kobayashi and M. Nitta, arXiv:1304.4737.
- [41] M. Kobayashi and M. Nitta, Torus knots as Hopfions, *Phys. Lett. B* **728**, 314 (2014).
- [42] L. D. Faddeev, Princeton Report No. IAS-75-QS70.
- [43] L. D. Faddeev and A. J. Niemi, Knots and particles, *Nature (London)* **387**, 58 (1997).
- [44] B. M. A. Piette, B. J. Schroers, and W. J. Zakrzewski, Multi-solitons in a two-dimensional Skyrme model, *Z. Phys. C* **65**, 165 (1995); Dynamics of baby skyrmions, *Nucl. Phys. B* **439**, 205 (1995).
- [45] T. Weidig, The baby Skyrme models and their multi-skyrmions, *Nonlinearity* **12**, 1489 (1999).
- [46] H. J. de Vega, Closed Vortices and the HOPF Index in Classical Field Theory, *Phys. Rev. D* **18**, 2945 (1978); A. Kundu and Y. P. Rybakov, Closed vortex type solitons with Hopf index, *J. Phys. A* **15**, 269 (1982).
- [47] J. Gladikowski and M. Hellmund, Static Solitons with Nonzero Hopf Number, *Phys. Rev. D* **56**, 5194 (1997).
- [48] R. A. Battye and P. M. Sutcliffe, Knots as Stable Soliton Solutions in a Three-Dimensional Classical Field Theory, *Phys. Rev. Lett.* **81**, 4798 (1998); Solitons, links and knots, *Proc. R. Soc. A* **455**, 4305 (1999).
- [49] J. Hietarinta and P. Salo, Ground State in the Faddeev-Skyrme Model, *Phys. Rev. D* **62**, 081701 (2000).
- [50] P. Sutcliffe, Knots in the Skyrme-Faddeev model, *Proc. R. Soc. A* **463**, 3001 (2007).
- [51] M. Kobayashi and M. Nitta, Winding Hopfions on $R^2 \times S^1$, *Nucl. Phys. B* **876**, 605 (2013).
- [52] F. Canfora, F. Correa, and J. Zanelli, Exact Multi-Soliton Solutions in the Four Dimensional Skyrme Model, *Phys. Rev. D* **90**, 085002 (2014).